Karlsruhe Institute of Technology

Damage in silica by hydroxyl generation: Behaviour at crack tips

T. Fett, G. Schell

KIT SCIENTIFIC WORKING PAPERS 87

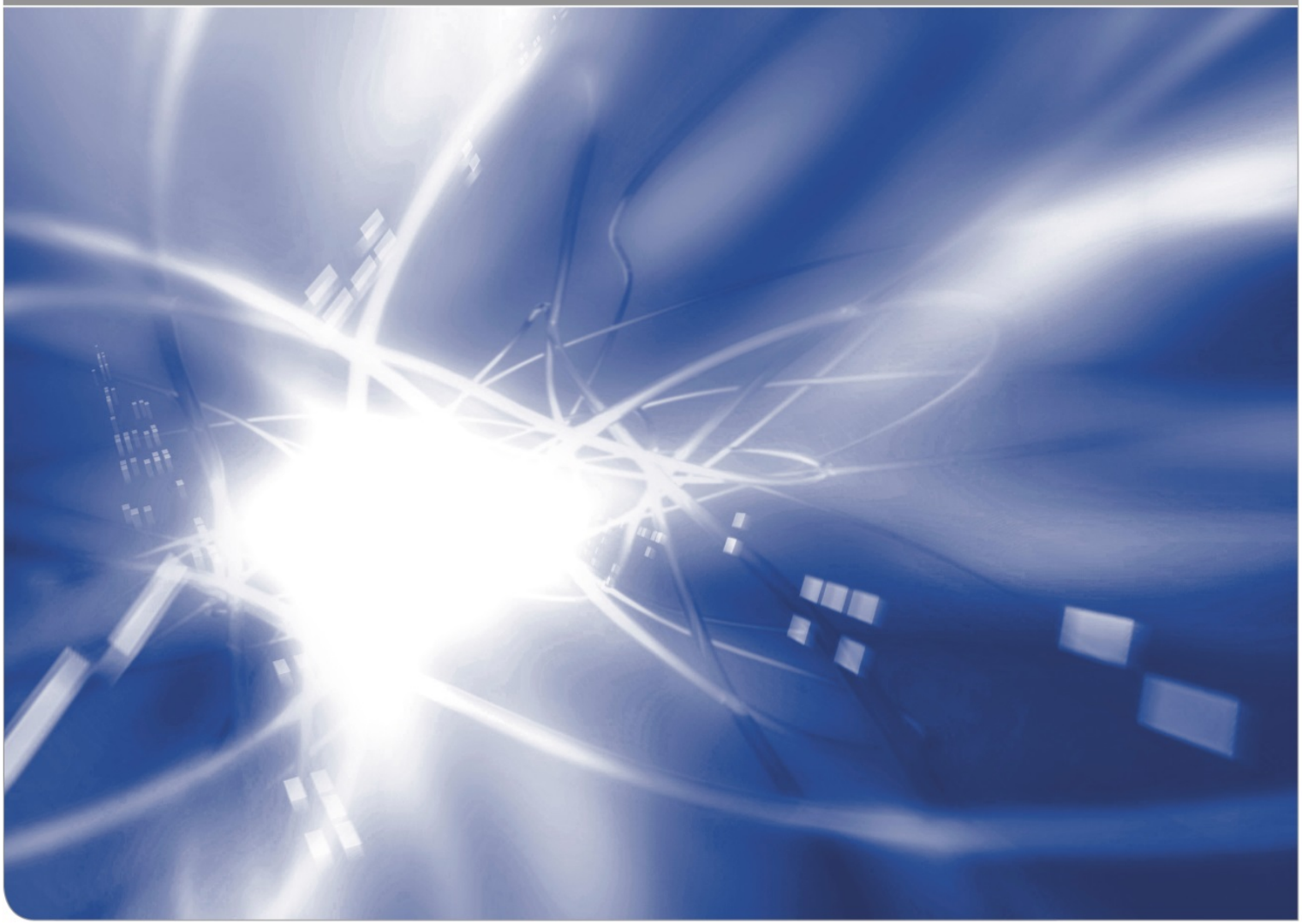

Institut für Angewandte Materialien, Karlsruher Institut für Technologie (KIT)

Impressum

Karlsruher Institut für Technologie (KIT)
www.kit.edu

2018

ISSN: 2194-1629

Abstract

Water diffusion into silica glass results in a zone where the water reacts with the SiO_2 structure and "damages" the originally intact SiO_2 rings. The consequence is a reduced Young's module. This effect must be strongly stress-enhanced at crack tips under the high near-tip stresses.

In this report the general influence on crack stability and local failure condition is addressed. The results give rise for subcritical crack growth in the sense of crack extension under applied stress intensity factors below the fracture toughness K_{Ic}. A threshold stress intensity factor for subcritical crack growth in silica can be concluded.

Contents

1 Damage by hydroxyl generation 1

2 Conclusions on the basis of the J-Integral 2

3 Slender notch approach 4

3.1 Notch radius from silica ring structure 4

3.2 Notch radius from theoretical strength 4

3.3 Notch radius from Theory of Critical Distance 5

4 Failure behaviour 6

4.1 Crack-growth resistance 6

4.2 General conclusion on crack stability 7

4.3 Hydroxyl concentration and K_{tip} as a function of K_{appl} 7

4.4 Crack stability 10

5 Reason for subcritical crack growth 11

Concluding remarks 12

References 13

1. Damage by hydroxyl generation

Water diffuses into silica glass as a molecule, occasionally reacting with the silica network according to the following equation:

$$\equiv\text{Si-O-Si}\equiv + H_2O \leftrightarrow \equiv\text{SiOH+HOSi}\equiv. \qquad (1.1)$$

The concentration of the hydroxyl water $S = [\equiv\text{SiOH}]$ is usually expressed in terms of the OH-concentration, [OH], whereas the concentration of the molecular water is given by $C = [H_2O]$.

When a hydroxyl has been formed, the initial silica ring is broken and the mechanical cohesion is weakened as is illustrated in Fig. 1. Such "defects" in the glass structure can be treated by using the damage variable D of continuum damage mechanics (Kachanov [1], Lemaitre [2]). This parameter is proportional to the density of micro-defects.

According to the postulate of strain equivalence by Lemaitre [3], the effective elastic modulus, E_D, decreases with increasing damage

$$E_D = E_0(1-D) \qquad (1.2)$$

where E_0 is the modulus of virgin glass. The damage variable D can be determined from module measurements via eq.(1.2).

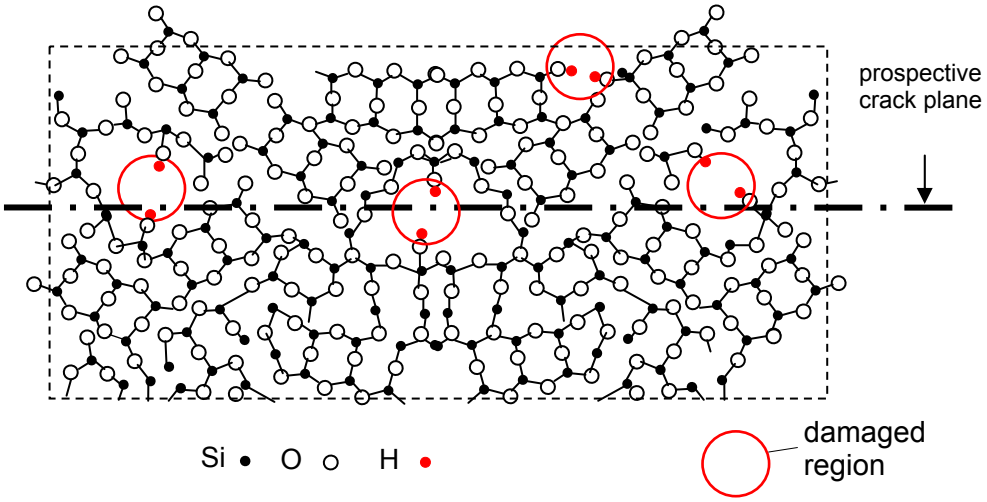

Fig. 1 Volume element of silica showing damage by bond breaking due to the water/silica reaction, third dimension ignored.

We assume in the following considerations that the damage is isotropic and considered to be of scalar nature. This is equivalent to the assumption of randomly orientated defects. We furthermore assume that nano-pores in SiO_2, caused by hydroxyl

generation, might behave like normal pores. Then also E remains isotropic and the damage D becomes dependent on the hydroxyl concentration:

In literature, there is experimental evidence for modulus decrease with increasing hydroxyl content. This can be seen from measurements of Young's modulus as a function of water content. Measurements on longitudinal sound velocities in silica specimens with different water content were reported by Fraser [4] and Le Parc et al. [5].

Analytical computations on the reduction of Young's modulus with porosity were carried out by Wang [6] for spherical pores. From the measurements and this model we could derive in [7]

$$\frac{E_D}{E_0} = 1 - D = \exp\left[- B_1 (S / S_{\max}) - \frac{B_2}{(1 - S / S_{\max})^{1/8}} \left(\frac{S}{S_{\max}} \right)^2 \right] \tag{1.3}$$

with the parameters B_1=5/3, $B_2 \cong 14/15$ and the maximum possible hydroxyl concentration $S_{\max}$. An approximate inverse representation is for instance

$$\frac{S}{S_{\max}} \cong \tfrac{3}{5} D + \tfrac{2}{5} D^3 \tag{1.4}$$

As a consequence of stresses acting during the silica/water reaction (1.1) the equilibrium is affected since the hydroxyl concentration is stress-dependent. This has been outlined in [8]. In order to allow a transparent derivation, swelling stresses may be neglected first. The hydroxyl concentration as a function of stress can be written

$$S = S_0 \exp[\gamma \sigma] \tag{1.5}$$

where S_0 is the hydroxyl concentration in the absence of any stress. At temperatures >500°C, the parameter γ reads for uniaxial loading [8]

$$\gamma = \frac{\kappa}{RT} \text{ with } \kappa = 14.4 (\text{cm}^3/\text{mol}) \tag{1.6}$$

2. Conclusions on the basis of the J-Integral

At crack tips under externally applied loads, the singular stresses must result in high hydroxyl concentrations and, consequently, high damage followed by a strong stress reduction. As long as a positive crack-tip stress intensity factor exists, $K_{\text{tip}} \geq 0$, also stress singularity must exist with $\sigma_{ij} \to \infty$. The hydroxyl concentration must reach its maximum possible value, $S_{\max}$, with the consequence that the damage must tend to $D \to 1$ and the Young's modulus must disappear at the tip, $E_D \to 0$. These consequences

make the occurrence of singular stresses and a crack-tip stress intensity factor at least questionable.

The problem will be discussed here by using the path-independence of the J-Integral by Rice [9]. For any time-independent material behaviour the fracture mechanics J-integral can be used as the loading parameter. It simply reads for linear-elastic materials

$$J = \frac{K^2(1-\nu^2)}{E} = G \tag{2.1}$$

where the right-hand side is also called the energy release rate G. Since the J-integral for any path around the crack tip is a parameter independent of the specially chosen path, its value must be the same for a path Γ far away from the tip (in the bulk) and the path Γ_D directly at the crack tip, i.e. in the damaged region as is illustrated in Fig. 2a

$$\frac{K_{appl}^2(1-\nu_0^2)}{E_0} = \frac{K_{tip}^2(1-\nu_D^2)}{E_D} \tag{2.2}$$

where E_D and ν_D are the elastic properties at the tip affected by water and K_{tip} is the true stress intensity factor present at the crack tip. For $\nu_D \cong \nu_0$

$$K_{tip} \cong K_{appl}\sqrt{\frac{E_D}{E_0}} \tag{2.3}$$

It has been shown by Merkle [10] that (2.3) also holds for slender notches.

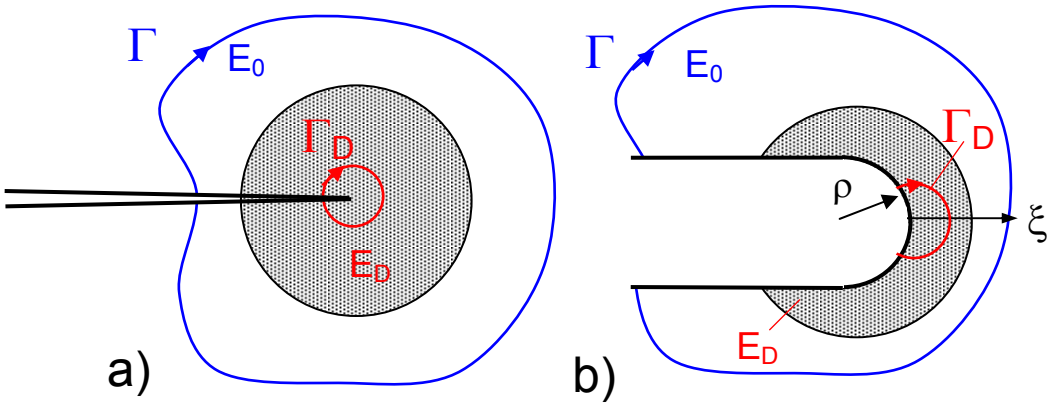

Fig. 2 a) Two J-integral paths around a crack tip; path Γ far away from the tip (blue) reflects the properties of the bulk material, path Γ_D (red) in the water-affected and damaged crack-tip region, b) paths for a notch.

Since in eq.(2.2) a finite value on the left-hand side is prescribed by the external loading, the right-hand side must be finite, too. For the crack tip it results due to $\sigma_{ij}\to\infty$ that: $S\to S_{max}$ and $E_D\to 0$. The disappearing denominator E_D requires that also the numerator must disappear. Consequently, it must hold $K=K_{tip}=0$ resulting in finite stresses. Under the assumption of finite notch radii, this problem vanishes.

3. Slender notch approach

3.1 Notch radius from silica ring structure

In a micro-structurally motivated approach, the crack tip region (Fig. 3a) is considered as a slender notch with root radius ρ in the order of the *average radius* of the SiO_2 rings, Fig. 3b. For such a notch, Wiederhorn et al. [11] suggested a crack-tip radius of $\boldsymbol{\rho = 0.5\ nm}$.

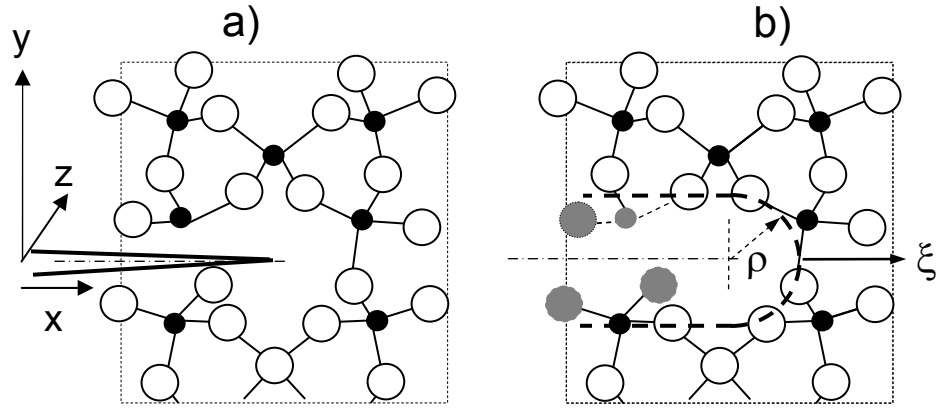

Fig. 3 a) Crack in silica terminating in a nano-pore, b) equivalent slender notch with a finite notch root radius ρ, grey molecules are mechanically inactive.

3.2 Notch radius from theoretical strength

Stresses at slender notches were given by Creager and Paris [12]. The stress component normal to the crack plane (the tangential stress $\sigma_t=\sigma_y$) is in distance ξ from the notch root (Fig. 4)

$$\sigma_y = \frac{2K}{\sqrt{\pi(\rho+2\xi)}}\frac{\rho+\xi}{\rho+2\xi} \tag{3.1}$$

The other stress components are

$$\sigma_x = \frac{2K}{\sqrt{\pi(\rho+2\xi)}}\frac{\xi}{\rho+2\xi} \tag{3.2}$$

$$\sigma_z = \frac{2\nu K}{\sqrt{\pi(\rho+2\xi)}} \tag{3.3}$$

Directly at the notch root, ξ=0, it holds for the maximum stress

$$\sigma_y = \sigma_{\max} = \frac{2K}{\sqrt{\pi\rho}}, \quad \sigma_z = \nu\sigma_y \tag{3.4}$$

The fracture toughness of silica is $K_{Ic} = 0.8$ MPa√m [13] and the theoretical strength is about [14]

$$\sigma_0 = \frac{E}{\pi} \cong 23\,\text{GPa} \tag{3.5}$$

as is in agreement with strengths up to 25GPa measured by Brambilla and Payne [15] on extremely thin silica fibers of about 60 nm radius.
The notch-root radius results then from the condition $\sigma_y=\sigma_0$ for $K=K_{Ic}$ as **ρ≅1.5 nm**.

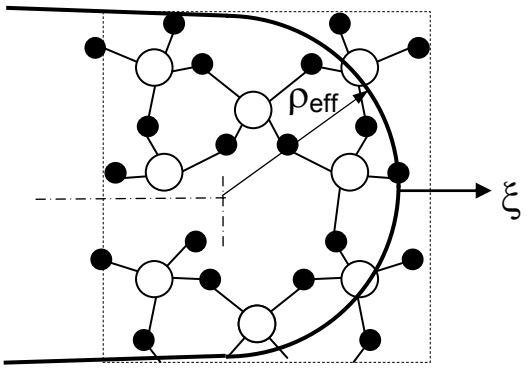

Fig. 4 Mechanically effective notch from theoretical strength.

3.3 Notch radius from Theory of Critical Distance

A third estimate of the root radius ρ can be obtained by use of a non-local approach. The location at which failure occurs can be computed by application of the "Theory of Critical Distances" (TCD) as was developed by Taylor [16, 17]. The TCD postulates that failure occurs when a distance dependent effective stress σ_{eff} exceeds the tensile strength σ_0.
The effective stress is in this approach the stress value σ_y in a distance of $\xi=L$ from the notch root, where the length L is given by

$$L = \frac{1}{2\pi}\left(\frac{K_{Ic}}{\sigma_0}\right)^2 \tag{3.6}$$

Introducing (3.6) and (3.5) into (3.1) and setting $\xi=L$ results in

$$\rho = \frac{(1+\sqrt{5})}{2\pi\sigma_0^2} K_{Ic}^2 \rightarrow \boldsymbol{\rho \cong 0.62\ \text{nm}} \tag{3.7}$$

This says that in the light of the TCD-approach the guess by Wiederhorn et al. [11] is a good estimate.
The failure location, L in Fig. 5, results from (3.6) and (3.7) as

$$L = \frac{1}{1+\sqrt{5}}\rho \cong 0.309\rho \tag{3.8}$$

with the maximum stress for ξ=0, σ_{max}, given by eq.(3.4), the stress at ξ=L results as

$$\sigma_{max} = \sqrt{2(\sqrt{5}-1)}\ \sigma_0 \cong 1.572\sigma_0 \tag{3.9}$$

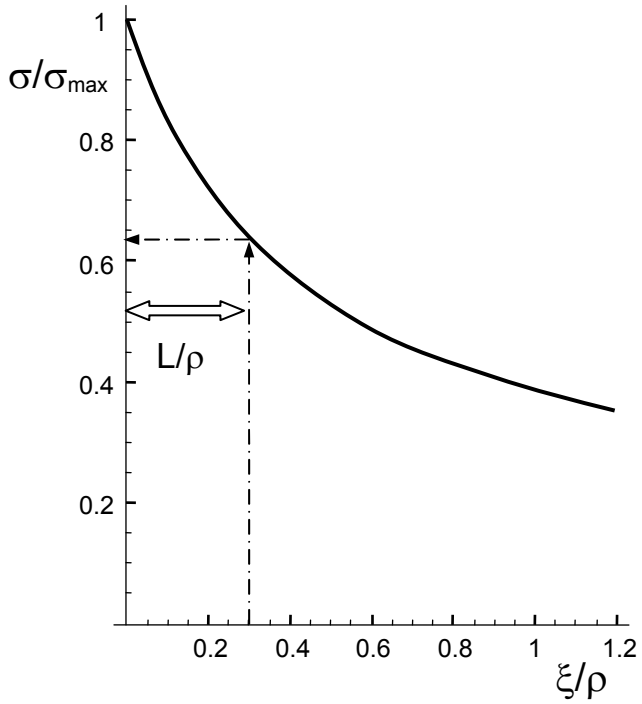

Fig. 5 Failure location ahead of a notch root according to the TCD by Taylor [16,17].

4. Failure behaviour

4.1 Crack-growth resistance

The damage variable D according to Lemaitre [3] can be interpreted as the part of the material cross-section that can no longer transmit forces. Consequently, the area that can carry load, A_D, is reduced to

$$A_D = A_0(1-D) \tag{4.1}$$

where A_0 denotes the total geometrical cross section subsuming damaged and un-damaged regions. The crack growth resistance G_c represents the energy necessary to split all bonds that are broken when the crack has passed the considered volume ele-

ment. Application of the damage variable yields for the crack growth resistance of the damaged material, $G_{c,D}$,

$$G_{c,D} = G_{c,0}(1-D) \tag{4.2}$$

($G_{c,0}$ = crack resistance for the undamaged material, D=0) or in terms of stress intensity factors

$$K_{c,D} = \sqrt{E_D\, G_{c,D}} = \sqrt{E_0(1-D)G_{c,0}(1-D)} = \underbrace{\sqrt{E_0 G_{c,0}}}_{K_{\mathrm{Ic}}}(1-D)$$

$$\Rightarrow \quad K_{c,D} = K_{\mathrm{Ic}}(1-D) \tag{4.3}$$

where $K_{c,D}$ is the reduced toughness of the damaged material and K_{Ic} the fracture toughness measured in fracture mechanics tests on the undamaged material.

4.2 General conclusion on crack stability

Crack extension in the absence of damage is governed by the condition that the applied stress intensity factor equals the fracture toughness, i.e.

$$K_{appl} = K_{\mathrm{Ic}} \tag{4.4}$$

In presence of hydroxyl water and damage at the crack tip, this relation has to be replaced by the *local* failure condition

$$K_{tip} = K_{\mathrm{Ic},D} \tag{4.5}$$

From eq.(4.5) a critical value of the applied stress intensity factor, $K_{\mathrm{appl,c}} \neq K_{\mathrm{Ic}}$, has to be concluded that after introducing eqs.(2.3) and (4.3) reads

$$K_{appl}\sqrt{1-D} = K_{\mathrm{Ic}}(1-D) \Leftrightarrow K_{appl,c} = K_{\mathrm{Ic}}\sqrt{1-D} \tag{4.6}$$

Equation (4.6) says that cracks with hydroxyl at the tip can propagate at stress intensity factors even below the fracture toughness, i.e.

$$K_{appl,c} \leq K_{\mathrm{Ic}} \tag{4.7}$$

with the equality sign only for D=0. Whereas eq.(4.4) governs *stable* crack extension, the condition (4.7) ensures the existence of *subcritical* crack propagation so far without information of time- and rate-effects.

4.3 Hydroxyl concentration and K_{tip} as a function of K_{appl}

In 4.2 we concluded the rather trivial result that a crack can grow even below fracture toughness K_{Ic} due to the local damage at the tip. Next, we will compute the local

hydroxyl concentration and the damage as a function of the externally applied stress intensity factor K_{appl}. For this purpose we first rewrite eq.(1.5) as

$$S = S_0 \exp\left[\gamma \frac{K_{tip}}{K_{\mathrm{Ic}}} \sigma_0 \right] \tag{4.8}$$

and then introduce eqs.(1.2) and (2.3)

$$S = S_0 \exp\left[\gamma \frac{K_{appl}}{K_{\mathrm{Ic}}} \sqrt{1 - D(S)}\, \sigma_0 \right] \tag{4.9}$$

The result is an implicit equation for the dependency $S(K_{\mathrm{appl}})$ since S occurs on both sides. This relation cannot be solved analytically. Therefore, we determine the inverse function, $K_{\mathrm{appl}}(S)$, according to

$$K_{appl} = \frac{K_{\mathrm{Ic}}}{\gamma \sigma_0 \sqrt{1 - D(S)}} \ln \frac{S}{S_0} \tag{4.10}$$

and invert this solution numerically by using spline interpolation functions. For graphical representation of $S(K_{\mathrm{appl}})$, the plot $K(S)$ can be produced simply by changing coordinates.

The near-tip stress state on the prospective plane of a crack is multiaxial with the Cartesian components

$$\sigma_z = \sigma_y \quad , \sigma_x = 2\nu\sigma_z \tag{4.11}$$

Here, σ_z is the stress normal on the prospective crack plane, σ_y the stress in crack propagation direction and σ_x the stress component parallel to the crack front. ν is Poisson's ratio, ν=0.17.

The hydrostatic stress, defined as

$$\sigma_h = \tfrac{1}{3}(\sigma_x + \sigma_y + \sigma_z) \tag{4.12}$$

is then

$$\sigma_h = \tfrac{2}{3}(1+\nu)\sigma_z \underset{\nu=0.17}{=} 0.78\sigma_z \tag{4.13}$$

Compared to the uniaxial tensile stresses addressed in [8] where $\sigma_h=\sigma_z/3$, this value is much closer to the purely hydrostatic stress state described by $\sigma_h/\sigma_z=1$ and is therefore much more appropriate for crack problems. In the following we therefore use purely hydrostatic stresses. As outlined in [18] this circumstance results in $\kappa \approx 5$ cm^3/mol.

The hydroxyl concentration S as a function of the applied stress intensity factor is plotted in Fig. 6a for room temperature with S_0= 0.0347 wt% [19] and differently chosen parameters κ in eq.(1.6). The crack-tip stress intensity factor is represented in Fig. 6b

versus the applied one. In this plot, the red arrows indicate the maximum values that can be computed from eq.(4.10) as

$$K_{tip,\max} = \frac{K_{Ic}}{\gamma\sigma_0} \ln \frac{S_{\max}}{S_0} \tag{4.14}$$

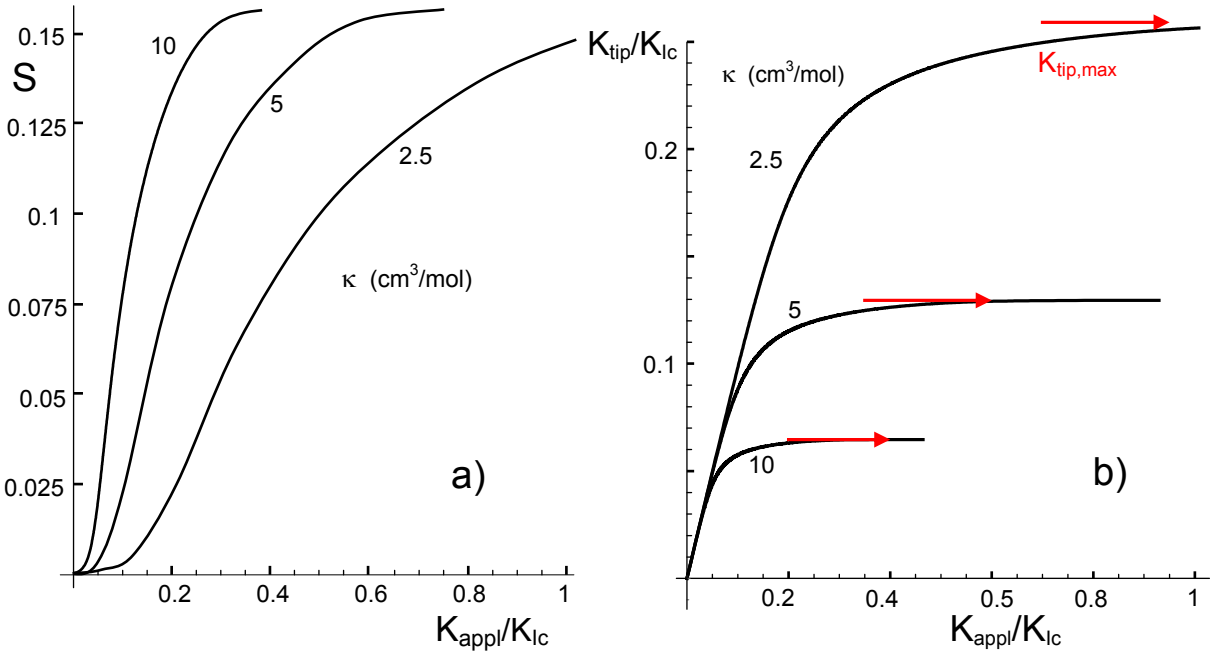

Fig. 6 a) Influence of the applied stress intensity factor K_{appl} on the hydroxyl concentration S, b) effect on the crack-tip stress intensity factor K_{tip} (red arrows indicate maximum K_{tip} according to eq.(4.14)).

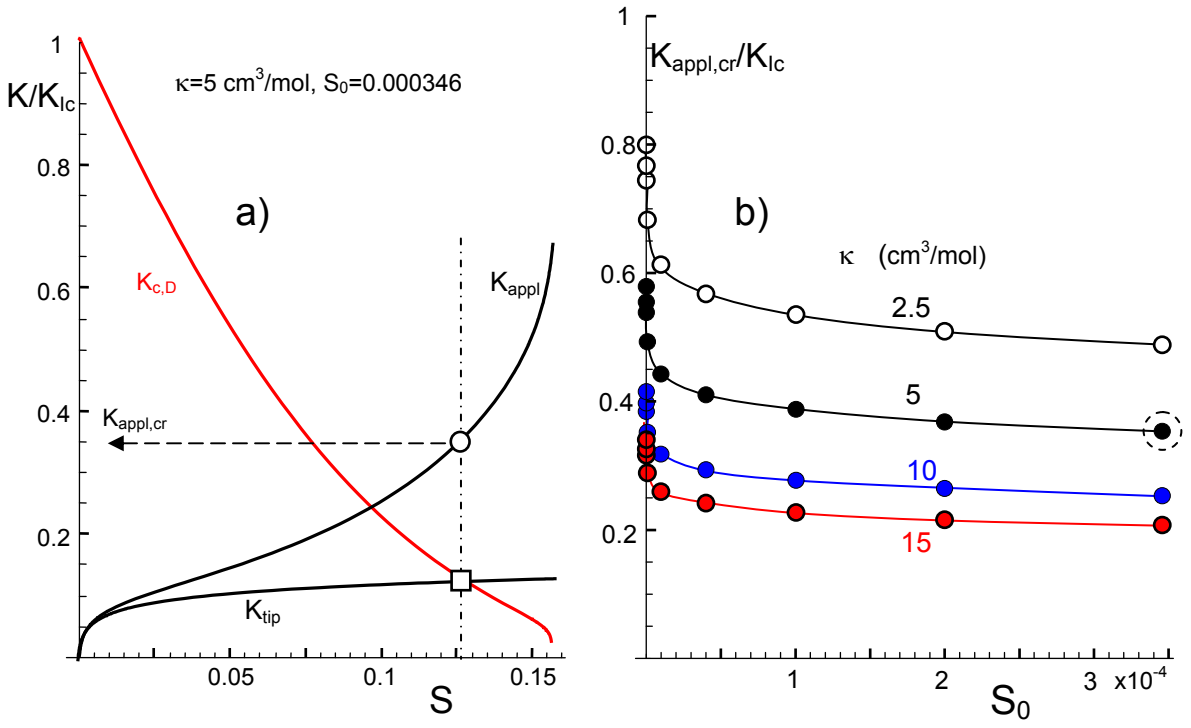

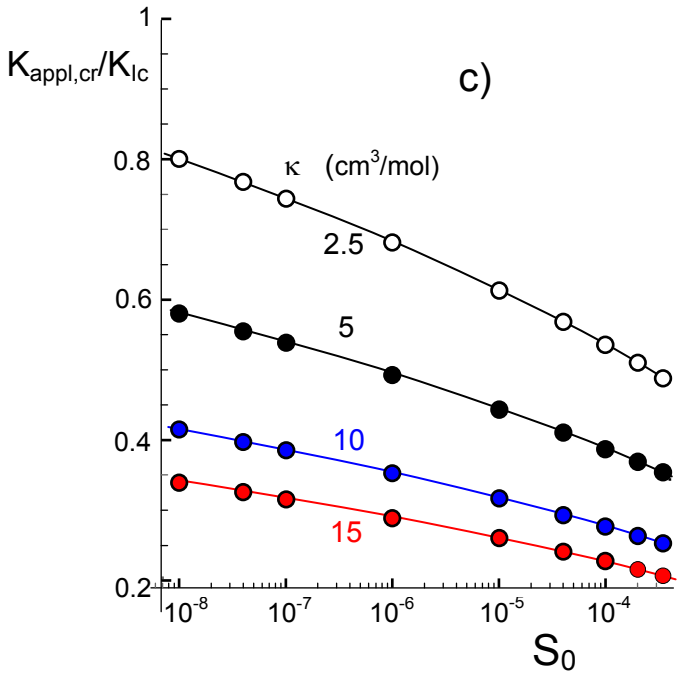

Fig. 7 a) Failure condition illustrated by the intersection of the crack-tip stress intensity factor K_{tip} with the curve for the critical value $K_{c,D}$, b) critical values of the applied stress intensity factor, $K_{appl,cr}$, obtained via the failure condition $K_{tip}=K_{c,D}$, c) results of b) in a semi-logarithmic plot.

Figure 7a illustrates the failure condition of the damaged material at a crack tip. The black curves show the applied and crack-tip stress intensity factors versus the hydroxyl concentration. The toughness is described by the red curves. The critical stress intensity factor according to eq.(4.3) is given by the condition $K_{tip}=K_{c,D}$, i.e. failure occurs at the intersection shown by the square, here at a critical hydroxyl concentration of $S_{cr}\cong 0.125$. The related value of the applied stress intensity factor is introduced in Fig. 7a as the circle. In Fig. 7b the critical values of the applied stress intensity factor, $K_{appl,cr}$, obtained via the failure condition $K_{tip}=K_{c,D}$, are plotted versus the hydroxyl concentration S_0.

4.4 Crack stability

Figure 7c shows the same result in a logarithmic representation. Figure 7b tells us for instance that the critical applied stress intensity factor for a water concentration of $S_0 =$ 0.0347 wt% would be in the case of $\kappa = 5$ cm^3/mol (encircled data point in Fig. 7b):

$$K_{appl,cr}=0.35\ K_{Ic}=0.28\ \text{MPa}\sqrt{\text{m}}.$$

Figure 8 illustrates the crack stability schematically for cracks of depth a. For an applied stress intensity factor, $K_{appl} > K_{appl,cr}$, spontaneous crack extension from the initial crack size a_0 must occur as is illustrated in Fig. 8 by the arrows. The perpendicular dashed lines represent the threshold stress intensity factor K_{th}. At values, $K_{appl}<K_{appl,cr}$, the material resists failure.

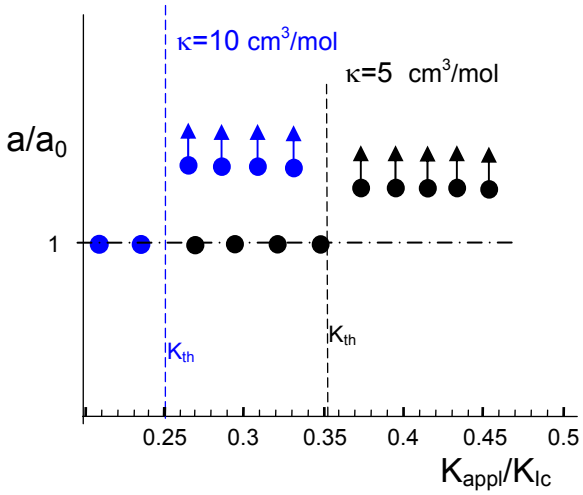

Fig. 8 Crack stability behaviour for κ=5 cm^3/mol and 10 cm^3/mol. Arrows indicate unstable extension.

5. Reason for subcritical crack growth

Cracks in silica modelled for instance by Fig. 4 or the model by Taylor [16, 17] describe failure in a certain distance $\xi=L$ below the "sharp" notch contour. When water at the tip comes in contact to silica, it has first to diffuse over the length L before it can cause failure. This needs of course a finite time. Neglecting stress-enhanced diffusivities and mass transfer coefficients h [20] the molecular water profiles $C(t)$ are schematically given in Fig. 9a (C_0=maximum concentration at the surface).

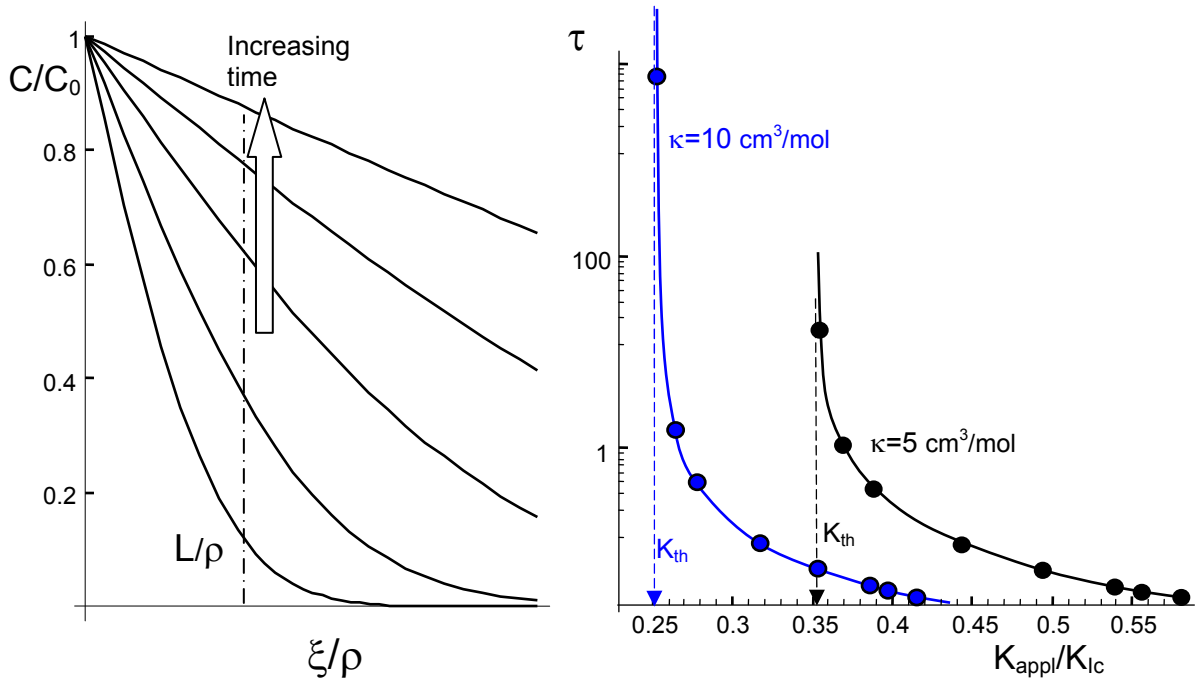

Fig. 9 Time-dependent water concentration at a crack tip, a) without stress-enhanced diffusivity, b) stress-enhanced diffusion included.

In Fig. 9b the normalized time τ, defined by here as

$$\tau \stackrel{def}{=} \frac{t\,D}{L^2} \tag{5.1}$$

is plotted versus K_{appl}/K_{Ic}. The time tends against infinity at the thresholds for $\kappa = 5$ and 10 cm^3/mol. Even in the case that local failure at $K_{appl,c}$ must occur, the time necessary for reaching the related water concentration must result in a delay of failure. The reciprocal time $1/\tau$ that is proportional to the crack-growth rate v of subcritical crack growth is shown in Fig. 10. With the fracture toughness of silica K_{Ic}=0.8 MPa√m [13], the threshold value for subcritical crack growth is introduced at K=0.28 MPa√m.

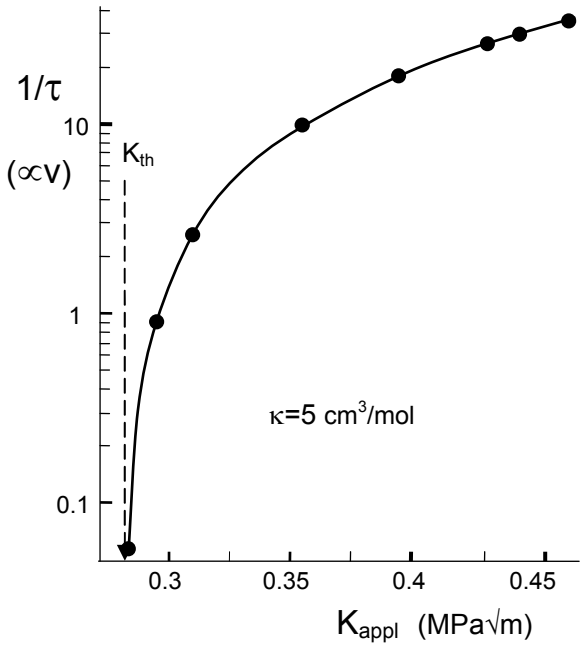

Fig. 10 Reciprocal normalized time characterizing crack growth rate v of subcritical crack growth.

Concluding remarks

There is so far much unpredictability that makes quantitative computations of the threshold value and the shape of the subcritical crack growth curve impossible without extensive additional studies. Only some points may be mentioned:

- So far, the parameter κ in eqs.(4.8-4.10) is unknown and had to be used as a free parameter. Its value of course must depend on the stress state for which uniaxial and hydrostatic stresses are limit cases.
- The diffusivity, affecting the time effects is stress-dependent. What the diffusivity in the damaged material is and in which way the activation volume for stress-enhancement depends on the damage are completely open questions.

- Furthermore, the entrance of water into the surface is unknown. Especially the questions, whether a *mass-transfer coefficient* [20] or *reaction parameter for a slow surface reaction* [21] exists at the freshly formed crack faces and how strong this parameter would depend on the damage have to be clarified.
- Last, it has to be emphasized that the reaction between silica and water is assumed to be in the equilibrium state. This simplifying assumption may be not necessarily fulfilled.

What we can say so far is that a threshold stress intensity factor for subcritical crack growth must exist even for silica.

References

1 L.M. Kachanov, Time of the rupture process under creep conditions, TVZ Akad Nauk S.S.R. Otd Tech. Nauk **8**(1958)

2 J. Lemaitre, Evaluation of dissipation and damage in metals, Proc. I.C.M. 1, Kyoto Japan (1971).

3 J. Lemaitre, How to use damage mechanics, Nuclear Engng. Design **80**(1984), 233-245.

4 D.B. Fraser, Factors Influencing the Acoustic Properties of Vitreous Silica, Citation: Journal of Applied Physics 39(1968), 5868-5878.

5 R Le Parc, C Levelut, J Pelous, V Martinez, B Champagnon, Influence of fictive temperature and composition of silica glass on anomalous elastic behavior *J. Phys.: Condens.* Matter **18**(2006), 7507-27.

6 J.C. Wang, Young's modulus of porous materials, J. Mater. Sci. **19**(1984), 801-808.

7 T. Fett, G. Schell, Damage in silica by hydroxyl generation described by Wang's theoretical data, Scientific Working Papers **85**, 2018, KIT Scientific Publishing, Karlsruhe.

8 S. M. Wiederhorn, G. Rizzi, S. Wagner, M. J. Hoffmann, and T. Fett, Stress-Enhanced Swelling of Silica: Effect on Strength, J. Am. Ceram. Soc. **99**(2016), 2956-63.

9 Rice, J.R., A path independent integral and the approximate analysis of strain concentration by notches and cracks, Trans. ASME, J. Appl. Mech. (1986), 379-386.

10 J. G. Merkle, An application of the J-integral to an incremental analysis of blunt crack behavior, Mechanical Engineering. Publications, London, 1991, 319-332.

11 S.M. Wiederhorn, E.R. Fuller, Jr. and R. Thomson, "Micromechanisms of crack growth in ceramics and glasses in corrosive environments," Metal Science, **14**(1980), 450-8.

12 Creager, M., Paris, P.C., Elastic field equations for blunt cracks with reference to stress corrosion cracking, Int. J. Fract. **3**(1967), 247-252.

13 S.M. Wiederhorn, Fracture surface energy of glass, J. Am. Ceram. Soc. **52** (1969), 99-105.

14 Silva, E. C. C. M.; Tong, L.; Yip, S.; Van Vliet, K. J. *Small* **2006**, *2*, 239–243.

15 G. Brambilla, D.N. Payne, The ultimate strength of glass silica nanowires, Nano Letters, **9**(2009), 831-835.

16 D. Taylor, Predicting the fracture strength of ceramic materials using the Theory of critical distances, Engineering Fracture Mechanics, 71 (2004) 2407.

17 D. Taylor, The Theory of Critical Distances: A New Perspective in Fracture Mechanics. Elsevier, Oxford, UK (2007).

18 G. Schell, G. Rizzi, T. Fett, Hydroxyl concentrations on crack surfaces from measurements by Tomozawa, Han and Lanford, Scientific Working Papers **82**, 2018, KIT Scientific Publishing, Karlsruhe.

19 S. M. Wiederhorn, G. Rizzi, G. Schell, S. Wagner, M. J. Hoffmann, T. Fett, Diffusion of water in silica: Influence of moderate stresses, J. Am. Ceram. Soc. **101**(2018), 1180-1190.

20 S.M. Wiederhorn, G. Rizzi, S. Wagner, M.J. Hoffmann, T. Fett, Diffusion of water in silica glass in the absence of stresses, J Am Ceram Soc. 100 (2017), 3895–3902.

21 R.H. Doremus, Diffusion of Reactive Molecules in Solids and Melts, Wiley, 2002, NewYork.

KIT Scientific Working Papers
ISSN 2194-1629

www.kit.edu